Biointerface Research in Applied Chemistry
Open-Access Journal (ISSN: 2069-5837)

*Article*
**Volume 13, Issue 3, 2023, 294**
https://doi.org/10.33263/BRIAC133.294

# Effect of Molybdenum Oxide on Structural Characteristics, Thermal Properties, and Chemical Dissolution of (50-*x*)$K_2O$-*x*$MoO_3$-50$P_2O_5$ Phosphate Glasses

**Asmae Er-Rafai [1], Mouloud El Moudane [1], Yasmina Alaoui [1], Mohamed Laourayed [1], M'hamed Taibi [2], Ismail Warad [3,4], Abdallah Guenbour [1], Abdelkabir Bellaouchou [1], Abdelkader Zarrouk [1,*]**

1 Laboratory of Materials, Nanotechnology and Environment, Faculty of Sciences, Mohammed V University in Rabat, Av. Ibn Battouta, P. O. Box 1014 Agdal-Rabat, Morocco
2 Laboratoire de Physico-chimie des Matériaux Inorganiques et Organiques (LPCMIO), Mohammed V University in Rabat, Ecole Normale Supérieure (ENS), Morocco
3 Department of Chemistry, AN-Najah National University, P.O. Box 7, Nablus, Palestine
4 Faculty of Pharmacy, Arab American University, P.O. Box 249, Jenin, Palestine
* Correspondence: azarrouk@gmail.com (A.Z.);

Scopus Author ID 36125763200
**Received: 3.03.2022; Accepted: 17.04.2022; Published: 12.07.2022**

**Abstract:** A new phosphate glass with the composition (50-x)$K_2O$-x$MoO_3$-50$P_2O_5$ was developed using the standard melt-quenching technique. X-ray powder diffraction was used to confirm the amorphous character of the glass samples. Differential scanning calorimetry was used to determine the glass transition temperature. The Tg values drop from 451°C for x = 0 mol% to 363°C for x = 40 mol%. Indeed, density, molar volume, and chemical dissolution are also studied. The results suggest that adding molybdenum oxide increases chemical dissolution and density while decreasing molar volume. Structural variations in the function of $MoO_3$ content were carried out by FT-IR and Raman spectroscopic data. Molybdenum oxide is assumed to break the structural glass network into pyrophosphate groups, making it more depolymerized and open. The microstructure of glass materials is examined by Scanning Electron Microscopy (SEM) coupled with an EDX. The elements that composed the samples were all identified.

**Keywords:** phosphate glasses; molybdenum; molar volume; chemical durability; glass transition temperature; FT-IR/Raman/SEM/EDX/XRD.



## 1. Introduction

Phosphate glasses have a low melting point, high UV transmission, and a high thermal expansion coefficient compared to ordinary silicate glasses [1-8]. The applications of phosphate glasses are growing in many technologies: radioactive waste vitrification [9], electrical conduction [10,11], glass-metal joints [12], as a solid-state laser source [13-18], and in Biocompatible Materials [19,20]. Unfortunately, the chemical durability of these glasses is relatively low, limiting their application [21,22]. On the other hand, they are useful for developing high energy density devices due to their high dielectric properties [23-28]. Recently, a lot of research has been conducted to improve the structural and chemical properties of phosphate glasses by inserting several glass formers and modifiers such as $TiO_2$, $V_2O_5$, $Al_2O_3$, $MoO_3$, $Cr_2O_3$, $Ta_2O_3$, $Sb_2O_3$, $As_2O_3$, etc., into the $P_2O_5$ glass network [29-34].

Molybdenum phosphate glasses were widely studied during the last years as they proved particularly beneficial for their ionic and electronic transport properties [35]. Molybdenum oxide-based glass materials were synthesized within diverse binary or ternary systems [35-41]. Xia Wu *et al*. [42] studied the lithium storage performance of $MoO_3$-$P_2O_5$ glasses as a cathode material for Li-ion batteries. The structure of PbO-$MoO_3$-$P_2O_5$ glasses was studied by Koudelka *et al*. [43] using Raman and NMR spectroscopy. The results showed a transformation of octahedral $MoO_6$ into tetrahedral $MoO_4$ units in the glasses with high $MoO_3$ content. Later, they studied BaO-$MoO_3$-$P_2O_5$ glasses [44]. Analysis of these glasses showed that the phosphate network had been depolymerized by incorporating molybdate units. In the last decade, Šubčík *et al*. [45] have determined the structure of ZnO-$MoO_3$-$P_2O_5$ glasses. For glasses rich in molybdenum oxide, the structure is characterized by forming several $MoO_6$ octahedra interconnected by corners and edges. L. Bih *et al*. [46] have investigated the redox stability of molybdenum in $Li_2O$-$MoO_3$-$P_2O_5$ phosphate glasses. The results have demonstrated that the structure does not influence the local environment of the Mo species.

As one of the best modifiers, potassium plays an important role not only in the melting process [47] but also used to modifying cations with low magnetic fields to improve their mechanical properties [48]. Characteristic studies of molybdophosphate glasses have been carried out by Selvaraj *et al*. [49]; they consider that molybdophosphate glasses consist of a network of [$MoO_{6/2}$] octahedra and [$POO_{3/2}$] tetrahedra shared in corners. In these glasses, the addition of $K_2O$ leads to a degradation of the network and creates a variety of defects. Thermal and chemical durability studies of binary $MoO_3$-$P_2O_5$ and ternary $K_2O$-$MoO_3$-$P_2O_5$ systems are reported by L. Abbas *et al*. [50], and the results obtained show that the reinforcement of the network increases at the same time the chemical durability and the thermal stability of the glasses studied. The study of the ternary system was carried out by varying the proportion of the oxide-forming $P_2O_5$.

Based on our investigation, there are no available data for potassium molybdenum phosphate glasses, where potassium oxide is substituted with molybdenum oxide by keeping the proportion of $P_2O_5$ fixed at 50 moles %. In this work, we aim to report the effect of $MoO_3$ in the structural, thermal, and chemical dissolution of the series $(K_2O)_{50-x}$-$(MoO_3)_x$-$(P_2O_5)_{50}$, x varies from 0 to 40% mol of molydbdenum oxide. X-ray powder diffraction was used to authenticate the amorphous character of the synthesized materials. Density (ρ), molar volume($V_M$) weight loss percentage and glass transition temperature (Tg) have been measured. The structural role of $MoO_3$ in these glasses has been discussed. The chemical dissolution of these glasses was tested in two solutions with different pH values. To evaluate the structure of these glasses as a function of the composition, we propose a structural study using FT-IR and Raman spectroscopy techniques. The microstructure of glassy materials is examined by Scanning Electron Microscopy (SEM) coupled with an EDX micro-analyzer.

## 2. Materials and Methods

### *2.1. Glass preparation.*

In this paper, the glasses studied have a composition given by the formula (50-x)$K_2O$-x$MoO_3$-50$P_2O_5$, where x is the molar percentage of molybdenum oxide ranging from 10 to 40 molar %; they were synthesized by the conventional melt-quenching method from reactive grade $NH_4H_2PO_4$, $(NH_4)_6Mo_7O_{24}$, $4H_2O$, and $K_2CO_3$. All batches were placed in an alumina crucible and treated for 2 hours at temperatures ranging from 200 to 500 degrees Celsius to

evaporate ammonia, water, and carbon dioxide, following which the temperature was gradually increased to 1100 degrees Celsius and held constant for half an hour. Melts have been rapidly cooled under air ambient to generate vitreous samples. The compositions synthesized and studied in the present work are regrouped in Table 1.

*2.2. X-ray diffraction.*

This technique was done according to the procedure of another work already published by Abdouni *et al*. [21] with λ=0.5418 nm in the 2 θ range between 10° and 70° at a scanning frequency of 2° per minute to verify the amorphous character of the materials generated in this investigation.

*2.3. Density and molar volume measurements.*

The Archimedes method was used to determine the density of the glass at room temperature using diethyl phthalate as an immersion solution. The density of a sample is determined by weighing it in air and then in diethyl phthalate. The density is calculated using the following formula:

$$\rho = \frac{w_{air} \times \rho_{ph}}{w_{air} - w_{ph}} \quad (1)$$

where $w_{air}$, $w_{ph}$, and $\rho_{ph}$ are respectively e weight of the sample in air, the weight of the sample in diethyl phthalate, and the density of diethyl phthalate are the three components of equation 1.

According to the relationship stated as, the molar volume $V_M$was computed from the molar mass M and ρ density: $V_M=M\times\rho^{-1}$.The error = ± 0.3 $cm^3mol^{-1}$.

*2.4. Thermal analysis.*

The glass transition temperatures were measured with a DSC- SETRAM apparatus at a heating rate of 10 °C.$min^{-1}$ in an argon atmosphere with an uncertainty of ± 5°C.

*2.5. Durability testing.*

With the aim of determining the chemical dissolution, we calculate the weight loss percentage (%) at each time point using the equation:

$$\text{weight loss (\%)} = \frac{m_0 - m_t}{m_0} \quad (2)$$

Where, $m_0$ is the initial mass of the glass block measured on day 0 and $m_t$ the mass at time point t. The experiments were carried out in two aqueous media for different pH (5.18 and 10.65) with an error = ± 0.01. The glasses were kept in the solutions at room temperature for 13 days. The weight loss of the samples at each time interval was measured with an uncertainty of 0.1 mg.

*2.6. Spectroscopic studies.*

The infrared analysis (IR) of the various samples studied was carried out using a Fourier transform infrared spectrometer (FT-IR) of the Bruker Platinum-ATR apparatus type operating in transmittance mode with a spectral measurement range extending from 400 to 1400 $cm^{-1}$.

Raman spectra were carried out for wavenumbers in the range 100-1400 $cm^{-1}$ on a Renishaw micro-Raman spectrometer RM1000 coupled to a He-Ne laser 19 mW, using the 632.8 nm line at room temperature.

*2.7. Scanning electron microscopy (SEM).*

To verify our glasses' microstructure, we used a Scanning Electron Microscopy (JEOL-JSM-IT-100) equipped with an EDX micro-analyzer.

## 3. Results and Discussion

*3.1. X-ray analysis.*

X-ray diffraction diffractogram at different concentrations of all potassium molybdenum phosphate glasses (Figure 1) demonstrates a large hump confirming their vitreous character.

**Table 1.** Nominal composition (mol %), density ρ ($g.cm^{-3}$), molar volume $V_M$ ($cm^3$. $mol^{-1}$) and glass transition temperature Tg (°C) of (50-x) $K_2O$-x$MoO_3$-50$P_2O_5$ glasses.

| x | $P_2O_5$ | $MoO_3$ | $K_2O$ | Density | Molar volume | Tg |
|---|---|---|---|---|---|---|
| **10** | 50 | 10 | 40 | 2.98 | 41.29 | 451 |
| **15** | 50 | 15 | 35 | 3.05 | 41.16 | 442 |
| **20** | 50 | 20 | 30 | 3.28 | 39.07 | 409 |
| **25** | 50 | 25 | 25 | 3.38 | 38.65 | 380 |
| **30** | 50 | 30 | 20 | 3.39 | 39.18 | 379 |
| **35** | 50 | 35 | 15 | 3.48 | 38.93 | 364 |
| **40** | 50 | 40 | 10 | 3.71 | 37.19 | 363 |

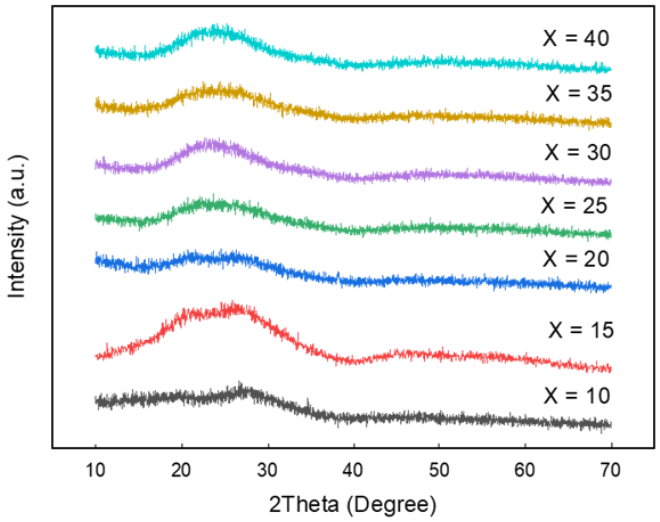


**Figure 1.** X-ray diffraction pattern for the seven compositions studied of (50-x) $K_2O$-x$MoO_3$-50$P_2O_5$ glasses.

*3.2. Density and molar volume.*

The glass transition is accompanied by a quick change in some properties, such as density [51]. In addition, the glassy network density (ρ) and molar volume ($V_M$) are affected by several parameters, namely the coordination number of the structure, the cross-linking density, and the interstitial space dimensionality [52].

The characteristic data of ρ, $V_m$, and $T_g$ have been regrouped in Table 1. The variations of density and molar volume with the composition of molybdenum oxide are shown in Figure

2. It appears in Table 1 and Figure 2 that the density of glasses increases progressively with $MoO_3$ content. Density increases from 2.98 $g.cm^{-3}$ for 10 mol % $MoO_3$ to 3.71 $g.cm^{-3}$ for 40 mol % $MoO_3$. This result can be explained by the larger molecular weights in the order $MoO_3$>$K_2O$. Similarly, this behavior may also be due to the difference in density between molybdenum (4.69 $g.cm^{-3}$) and oxide potassium oxide (2.35 $g.cm^{-3}$). Furthermore, the molar volume decreases when $K_2O$ is replaced by $MoO_3$. This trend could be assigned to the fact that the atomic radius of potassium is larger than those of molybdenum. Thus, this result could also be explained by replacing $K_2O$, which has a high molar volume, with $MoO_3$, which has a low molar volume. However, the molar volume shows an unusual variation for glasses containing 30 and 35 mol % of molybdenum oxide. This change could be due to a rearrangement of the structural units forming the vitreous network [43,45,49].

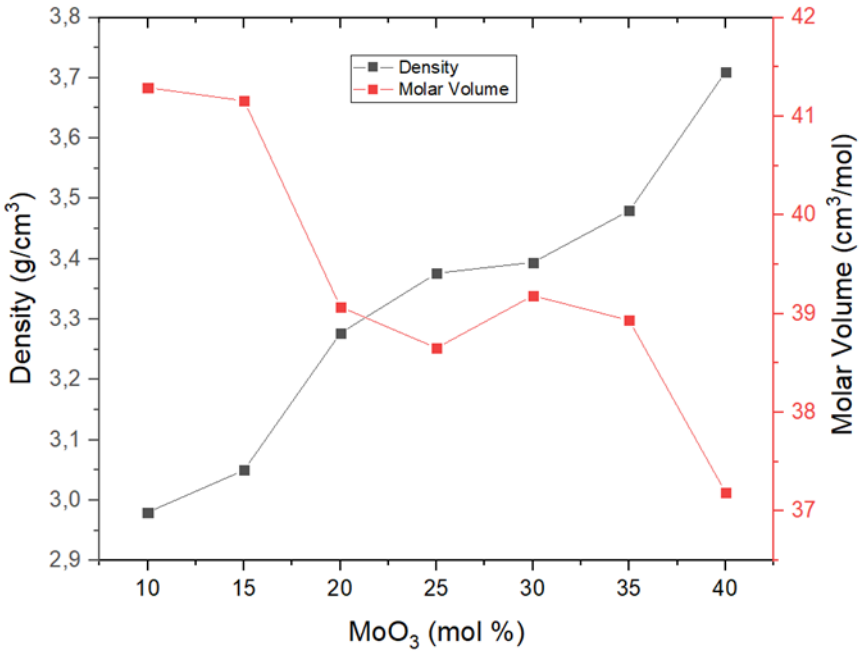


**Figure 2.** Density and molar volume of (50-x)$K_2O$-x$MoO_3$-50$P_2O_5$ glasses function of %$MoO_3$ concentration.

*3.3. DSC study.*

Figure 3 shows characteristic traces of differential scanning calorimetry analysis of the glasses under investigation. The values of the glass transition temperature (Tg) of the elaborated glasses according to the $MoO_3$ content are summarized in Table 1 and presented in Figure 4.

From the data shown in Table 1 and Figure 4, it can be seen that increasing the molybdenum oxide concentration in these glasses decreased the glass transition temperature, where we observed an increase in Tg. We supposed that the structure of the glass network is the main cause for the lowering of the glass transition temperature. We can admit that the substitution of $K_2O$ by $MoO_3$ causes a relaxation of the vitreous network, which leads to generating a more open structure, besides a possible change in the molybdenum's environment [43,45,49]. Thus, the decrease of Tg by adding $MoO_3$ has been observed by Abbas *et al*. [50] in the binary x$MoO_3$-(1-x)$P_2O_5$ glasses for a P/Mo ratio of more than 2. Furthermore, as shown in Figure 3, the endothermic peaks corresponding to Tg do not appear in the temperature range investigated, particularly for glasses with $MoO_3$ compositions ranging from 10% to 30%. This result clearly illustrates that above 700°C, the exothermic peak concerning crystallization will

be observed. As a result, the Tc-Tg difference (stability factor) will become more important, preventing crystallization and making the glasses thermally stable.

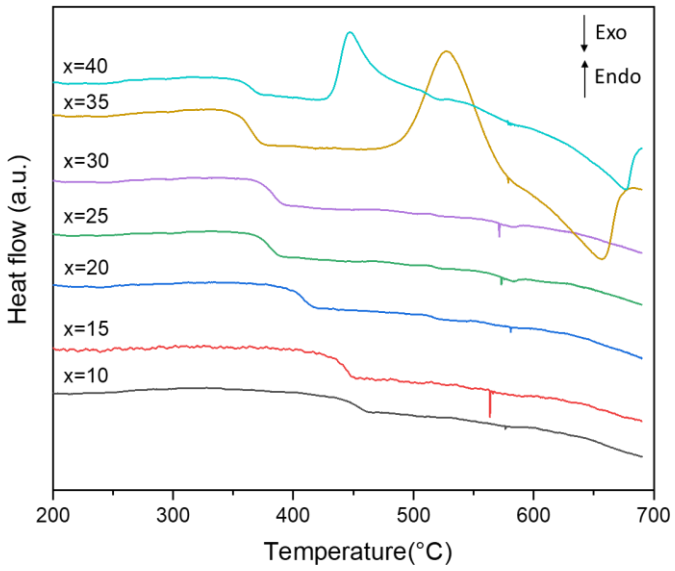


**Figure 3.** Thermograms DSC of (50-x)$K_2O$-x$MoO_3$-50$P_2O_5$ glasses.

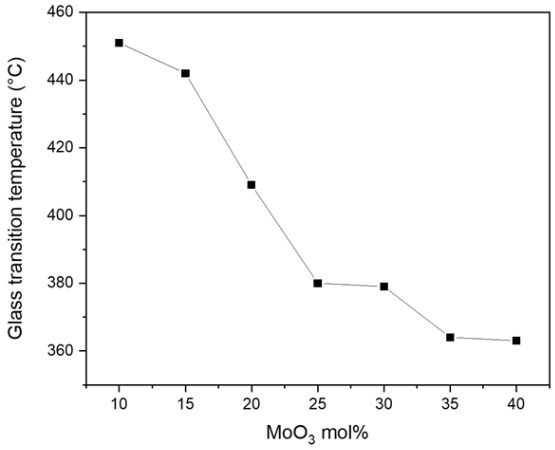


**Figure 4.** Evolution of glass transition temperature in function of $MoO_3$ mol% concentration in (50-x) $K_2O$-x$MoO_3$-50 $P_2O_5$ glasses.

*3.4. Chemical dissolution.*

We assessed the impact of the addition of molybdenum oxide on the chemical durability of our phosphate glasses. The chemical dissolution results of ternary (50-x) $K_2O$-x$MoO_3$-50$P_2O_5$ glasses expressed in weight loss with immersion time in two distinct pH media (5.18 and 10.65) are presented in Figure 5.

Adding molybdenum oxide in both aqueous solutions with pH values of 5.18 and 10.65 continually stimulates the chemical dissolution, especially when the amount of $MoO_3$ is higher than 15 mol %. On the other hand, for $MoO_3$ contents below 15 mol%, the glass dissolution is moderate, and the evolution tends to be linear. It can be noted that the evolution mass losses percentage is similar in the two aqueous media. However, more accentuated losses are observed in a basic medium (pH=10.65) than in an acid medium (pH=5.18). This behavior could be due to the pH of the solution. Replacing the stronger P-O-P bonds with the weakest P-O-Mo bonds [15] reduces the bond strength of the glass network and significantly accelerates the hydrolysis of P-O-Mo in both solutions. Thus, the chemical dissolution increases progressively. They

suggested that the gradual dissolution was due to replacing P–O–P bonds with the easily hydrolyzable P-O-Mo bonds and the decreased cross-linking between the phosphate chains. This result suggests that molybdenum oxide could act as a glass network modifying oxide in the presently studied glasses. This conclusion confirms those obtained by DSC analysis.

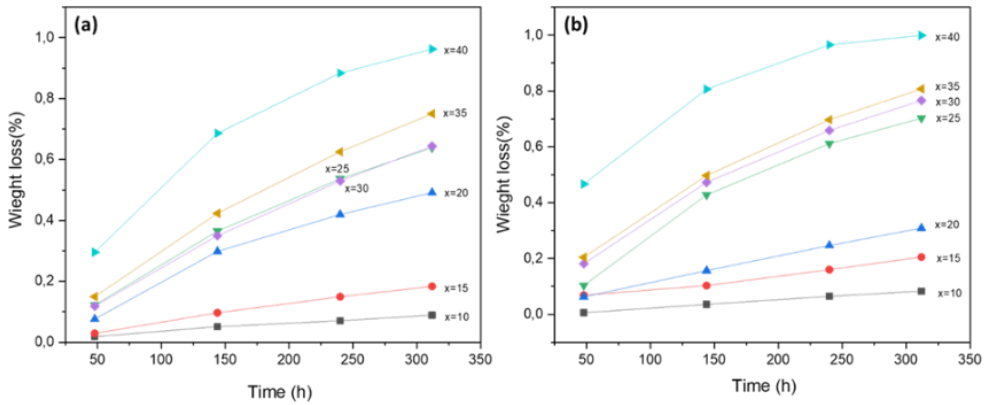


**Figure 5.** Weight loss (%) as a function of the immersion time in two solutions (a) pH =5.18 and (b) pH =10.65 of (50-x)$K_2O$-x$MoO_3$-50$P_2O_5$ glasses.

*3.5. FT-IR and Raman study.*

The IR spectra of the studied glasses with different proportions of $MoO_3$ in the frequency interval ranging from 400 $cm^{-1}$ to 1400 $cm^{-1}$ are presented in Figure 6, we attribute the different absorption bands found based on the literature research.

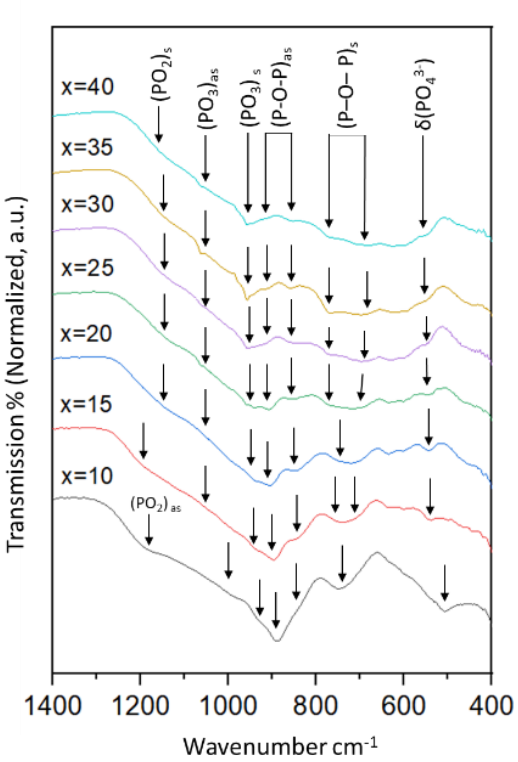


**Figure 6.** Infrared absorption spectra for a series of (50-x)$K_2O$-x$MoO_3$-50$P_2O_5$glasses.

The asymmetric and symmetric $\nu_{as}$ ($PO_2$) and $\nu_s$ ($PO_2$) stretching modes are centered at 1200 $cm^{-1}$ and 1130 $cm^{-1}$, respectively [53,31], whereas the asymmetric and symmetric $\nu_{as}$ ($PO_3$) and $\nu_s$ ($PO_3$) stretching vibrations are centered at 1050 $cm^{-1}$ and 980 $cm^{-1}$, respectively [1,54,55]. The absorption bands observed at 950-850 $cm^{-1}$are due to the $\nu_{as}$ of P-O-P groups,

and the bands remarked at 750-680 $cm^{-1}$ are associated with the $\nu_s$ of P-O-P groups in $PO_4$ structural units [56]. The vibration at 545 $cm^{-1}$ is attributed to the deformation vibration (δ) of $P-O^-$ in $PO_4^{3-}$ groups [51]. From figure 6, it can be seen that the intensity of $\nu_{as}$(POP) and $\nu_s$(POP) decreases with the increase in the percentage of $MoO_3$; this suggests that the P-O-P bonds are disturbed by $MoO_3$ [39,44]. Indeed, the band's intensity, located around 1200 $cm^{-1}$, decreases continually with the addition of molybdenum.

In the frequency range 100-1400 $cm^{-1}$, Figure 7 displays the Raman spectra of the examined $(50-x)K_2O-xMoO_3-50P_2O_5$ phosphate glasses with the addition of $MoO_3$. Band assignments for glasses are in good agreement with the data reported in the literature. The Raman spectrum recorded for glass containing 10 mol % of $MoO_3$ are the $PO_3$ asymmetric stretching vibration band $\nu_{as}$ ($PO_3$) at 1100 $cm^{-1}$[57], the $\nu_s$($PO_3$) groups at 950 $cm^{-1}$ [54], the $\nu_{as}$ of POP groups at 900-850 $cm^{-1}$ [58], the $\nu_s$ of POP groups at 750 $cm^{-1}$ [59] and the deformation vibration (δ) of $P-O^-$ in $PO_4^{3-}$ groups [55,57,60] at 400 $cm^{-1}$. The phosphate chain framework deformation vibrations and the deformation vibrations of $PO_3$ are linked to frequencies below 280 $cm^{-1}$.

The addition of $MoO_3$ causes many spectral modifications. The band located at 1100 $cm^{-1}$ disappeared when the concentration of $MoO_3$ was higher than 15 mol %. This change is probably due to the disruption of P-O-P bridges and phosphate chain depolymerization, which create phosphate dimers [44,61]. Indeed, the Raman spectra revealed that as the amount of $MoO_3$ increases, the asymmetric and symmetric bands of the P-O-P stretching mode move to lower frequencies. These results can be attributed to the decrease in the covalent character of P-O-P bonds, showing that the P-O-P bonds weaken when potassium is replaced by molybdenum [44].

On the other hand, the intensity of the $PO_3$ symmetric stretching vibration band decreases sharply by adding $MoO_3$. This behavior is due to the modifying effect of this oxide, thus causing a rupture and a weakening of the P=O bond strength. This result follows those obtained in the FT-IR spectroscopy, DSC investigation, and chemical dissolution. On the other hand, we can conclude that molybdenum oxide can play as a glassy network modifying oxide in the composition of these glasses [43-45].

Two specific bands at 900 and 750 $cm^{-1}$ associated with symmetric and asymmetric vibrations of the P-O-P bond, respectively [60], follow the existence of pyrophosphate units in these glassy materials.

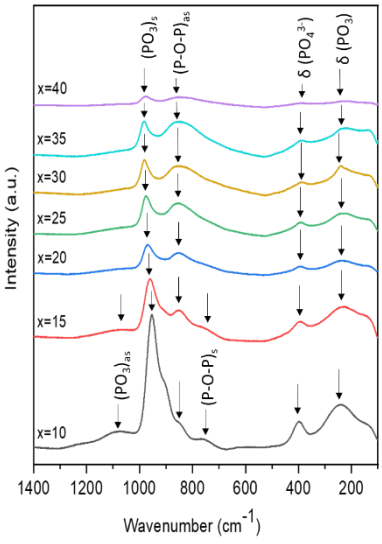


**Figure 7.** Raman spectra of $(50-x)K_2O-xMoO_3-50P_2O_5$ glasses.

*3.6. SEM study.*

Figure 8 shows the SEM images of two glass compositions $40K_2O$-$10MoO_3$-$50P_2O_5$ and $10K_2O$-$40MoO_3$-$50P_2O_5$, with different magnifications (x2500, x5000, and x10000). We can observe that the morphology is massive and compact, and there is no exact shape (A, B, C, E, F, and G). The EDX data collected at an average surface location are illustrated in Figure 8 (D and H). The composition of the synthesized samples was confirmed by identifying all of the elements that constituted the samples. According to SEM data, molybdenum oxide significantly impacts the texture and probably the physicochemical properties of the glasses investigated.

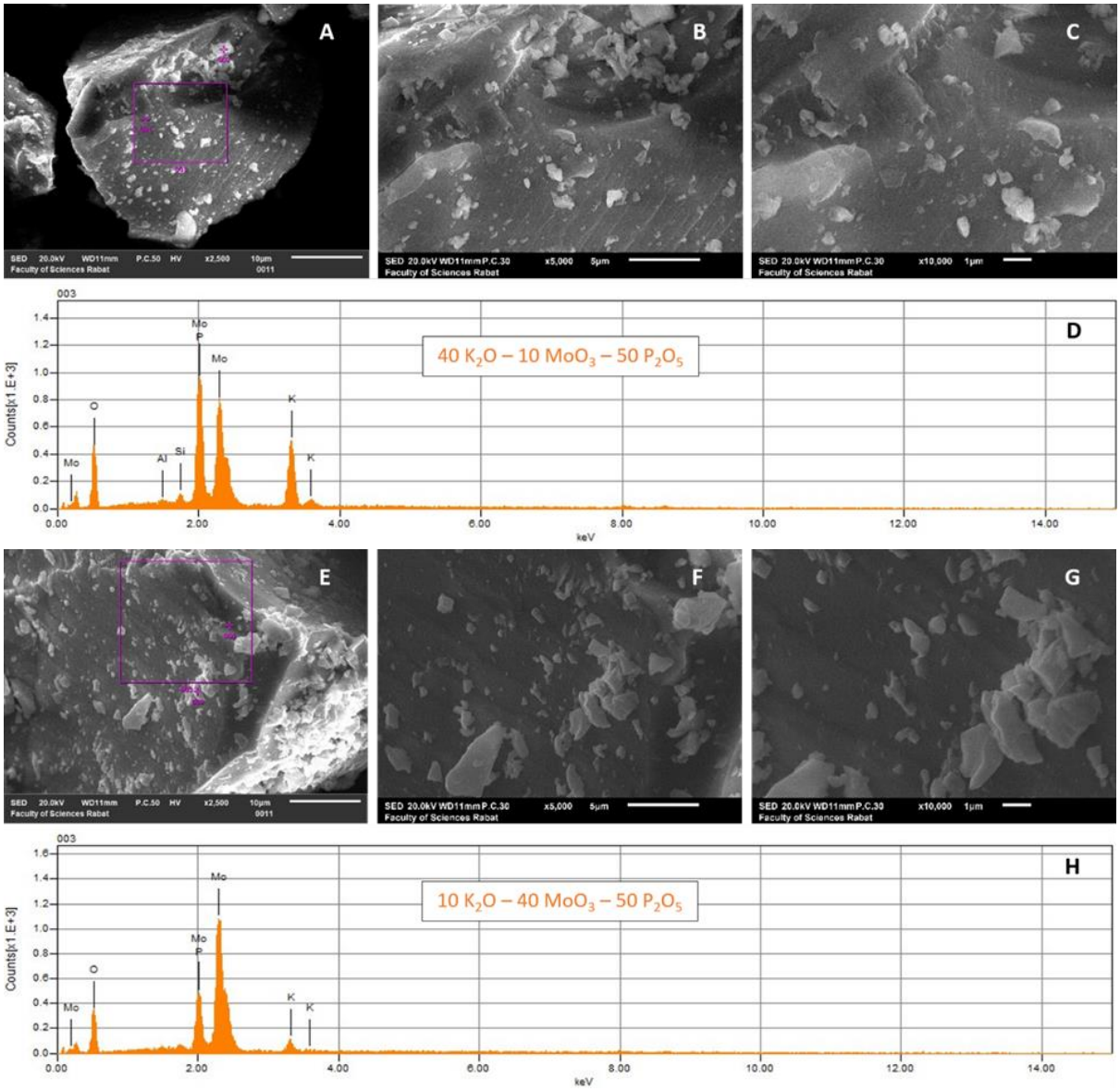


**Figure 8**. SEM image and EDS (A, B, C, and D) of $40K_2O$-$10MoO_3$-$50P_2O_5$ glassy and (E, F, G, and H) of $10K_2O$-$40MoO_3$-$50P_2O_5$ glassy.

## 4. Conclusions

The $(50\text{-}x)K_2O$-$xMoO_3$-$50P_2O_5$ glasses series was prepared using the traditional melt quenching method with $0 \leq x \leq 40$ mol %. When potassium oxide is replaced with molybdenum oxide, the vitreous network changes, this explains why the glass transition temperature reduces, and the density rises when $MoO_3$ is added. The results obtained are supported by measurements

of the chemical dissolution of the glasses investigated in two media of different pH (5.18 and 10.65). When $MoO_3$ is introduced, the glass network structure is broken into pyrophosphate units, as shown by IR and Raman spectroscopy. The presence of symmetric and asymmetric vibrations of the P-O-P Bridge could explain the existence of these groups. These studies, these studies show that molybdenum oxide may act as a glass network modifier.

## Funding

This research received no external funding.

## Acknowledgments

We thank all our colleagues.

## Conflicts of Interest

The authors declare no conflict of interest.

## References

1. Zhu, D.; Zhou, W.; Zhao, H. Glass formation in the $PbBr_2$-$PbCl_2$-$PbF_2$-PbO-$P_2O_5$ system. *Journal of Non-Crystalline Solids* **2000**, *270*, 278–282, https://doi.org/10.1016/S0022-3093(00)00065-X.
2. Reis, S.T.; Karabulut, M.; Day, D.E. Chemical durability and structure of zinc-iron phosphate glasses. *Journal of Non-Crystalline Solids* **2001**, *292*, 150–157, https://doi.org/10.1016/S0022-3093(01)00880-8.
3. Subbalakshmi, P.; Veeraiah, N. Study of CaO-$WO_3$-$P_2O_5$ glass system by dielectric properties, IR spectra and differential thermal analysis. *Journal of Non-Crystalline Solids* **2002**, *298*, 89–98, https://doi.org/10.1016/S0022-3093(01)01039-0.
4. Karakassides, M.A.; Saranti, A.; Koutselas, I. Preparation and structural study of binary phosphate glasses with high calcium and/or magnesium content. *Journal of Non-Crystalline Solids* **2004**, *347*, 69–79, https://doi.org/10.1016/j.jnoncrysol.2004.08.111.
5. Jermoumi, T.; Hafid, M.; Niegisch, N.; Mennig, M.; Sabir, A.; Toreis, N. Properties of (0.5-x)Zn-x$Fe_2O_3$-0.5$P_2O_5$ glasses. *Materials Research Bulletin* **2002**, *37*, 49–57, https://doi.org/10.1016/S0025-5408(01)00797-8.
6. Muñoz-Quiñonero, M.; Azkargorta, J.; Iparraguirre, I.; Jiménez-Riobóo, R.J.; Tricot, G.; Shao, C.; Muñoz, F.; Fernández, J.; Balda, R. Dehydroxylation processing and lasing properties of a Nd alumino-phosphate glass. *Journal of Alloys and Compounds* **2022**, *896*, https://doi.org/10.1016/j.jallcom.2021.163040.
7. Ramakrishna, P.; Padhi, R.K.; Mohapatra, D.K.; Jena, H.; Panigrahi, B.S. Structural characterization, $Gd^{3+}$ → $Eu^{3+}$ energy transfer and radiative properties of Gd/Eu in codoped $Li_2O$–ZnO–SrO–$B_2O_3$–$P_2O_5$ glass. *Optical Materials* **2022**, *125*, https://doi.org/10.1016/j.optmat.2022.112060.
8. Abouhaswa, A.S.; Tekin, H.O.; Araz, A.; Kavaz, E. Refinement of optical/structural features and neutron/gamma-ray protecting capability of $P_2O_5$–$Li_2O$–BaO phosphate glass system by adding Bi2O3. *Progress in Nuclear Energy* **2022**, *145*, https://doi.org/10.1016/j.pnucene.2021.104114.
9. Bergo, P.; Reis, S.T.; Pontuschka, W.M.; Prison, J.M.; Motta, C.C. Dielectric properties and structural features of barium-iron phosphate glasses. *Journal of Non-Crystalline Solids* **2004**, *336*, 159–164, https://doi.org/10.1016/j.jnoncrysol.2004.02.008.
10. Kumar, S.; Vinatier, P.; Levasseur, A.; Rao, K.J. Investigations of structure and transport in lithium and silver borophosphate glasses. *Journal of Solid State Chemistry* **2004**, *177*, 1723–1737, https://doi.org/10.1016/j.jssc.2003.12.034.
11. López-Grande, A.; Dagupati, R.; Galán del Sastre, P.; Muñoz, F. Ionic conductivity of $Li_2O$–$P_2O_5$ glasses from thermodynamic modeling of their chemical structure. *Journal of the American Ceramic Society* **2021**, *104*, 5625–5635, https://doi.org/10.1111/jace.17962.
12. Wei, T.Y.; Hu, Y.; Hwa, L.G. Structure and elastic properties of low-temperature sealing phosphate glasses. *Journal of Non-Crystalline Solids* **2001**, *288*, 140–147, https://doi.org/10.1016/S0022-3093(01)00612-3.
13. Alhasni, B. Insight into the structure of magnesium and sodium mixed phosphate glasses: A molecular dynamics study. *Journal of Non-Crystalline Solids* **2022**, *578*, https://doi.org/10.1016/j.jnoncrysol.2021.121338.
14. Abdel Wahab, E.A.; El-Maaref, A.A.; Shaaban, K.S.; Börcsök, J.; Abdelawwad, M. Lithium cadmium phosphate glasses doped $Sm^{3+}$ as a host material for near-IR laser applications. *Optical Materials* **2021**, *111*, https://doi.org/10.1016/j.optmat.2020.110638.

15. Es-Soufi, H.; Bih, L. Effect of TiO2 on the chemical durability and optical properties of Mo-based phosphate glasses. *Journal of Non-Crystalline Solids* **2021**, *558*, https://doi.org/10.1016/j.jnoncrysol.2021.120655.
16. Naseer, K.A.; Marimuthu, K.; Mahmoud, K.A.; Sayyed, M.I. The concentration impact of Yb3+ on the bismuth boro-phosphate glasses: Physical, structural, optical, elastic, and radiation-shielding properties. *Radiation Physics and Chemistry* **2021**, *188*, https://doi.org/10.1016/j.radphyschem.2021.109617.
17. Sreedhar, V.B.; Doddoji, R.; Kumar, K.K.; Reddy, V.; Reddy, M. A study of NIR emission and associated spectroscopic properties of $Nd^{3+}$: $P_2O_5$ + $K_2O$ + $Al_2O_3$ + $ZnF_2$ glasses for 1 . 06 μ m laser applications. *Journal of Non-Crystalline Solids* **2020**, *2*, https://doi.org/10.1016/j.jnoncrysol.2020.120521.
18. Campanella, C.; Ieee, S.M.; Guttilla, A.; Morana, A.; Ieee, M.; Michele, V. De; Muller, C.; Ieee, S.M.; Aubry, M.; Ieee, S.M.; Mady, F.; Marin, E.; Ouerdane, Y.; Boukenter, A.; Benabdesselam, M. Photobleaching Effect on Infrared Radiation- Induced Attenuation of Germanosilicate Optical Fibers at MGy dose levels. *IEEE Transactions on Nuclear Science* **2021**, *9499*, 1688–1693, https://doi.org/10.1109/TNS.2021.3068829.
19. Dias, A.G.; Skakle, J.M.S.; Gibson, I.R.; Lopes, M.A.; Santos, J.D. In situ thermal and structural characterization of bioactive calcium phosphate glass ceramics containing $TiO_2$ and MgO oxides: High temperature - XRD studies. *Journal of Non-Crystalline Solids* **2005**, *351*, 810–817, https://doi.org/10.1016/j.jnoncrysol.2005.01.060.
20. Singh, J.; Kumar, V.; Vermani, Y.K.; Singh, T. Evaluation of the physical, structural, thermal, and advanced radiation absorption characteristics of $SiO_2$–$Na_2O$–$K_2O$–$P_2O_5$–CaO bioactive glasses. *Journal of Physics and Chemistry of Solids* **2021**, *159*, https://doi.org/10.1016/j.jpcs.2021.110271.
21. El Abdouni, I.; Krimi, S.; Oudadesse, H. The Effects of Silicon Oxide on the Structure, Physical Chemistry Properties, and Bioactivity of Phosphate Glasses Containing Sodium, Strontium, and Titanium Oxides. *Physical Chemistry Research* **2022**, *10*, 1–12, https://doi.org/10.22036/PCR.2021.271462.1881.
22. Algradee, M.A.; Elbashar, Y.H.; Alwany, A.B.; Hassan, H.H.; El-Mallawany, R. Impact of Yb2O3 on the physical, bonding, dispersion and dielectric properties of $Li_2O$–ZnO–$P_2O_5$ glasses. *Materials Science in Semiconductor Processing* **2022**, *140*, https://doi.org/10.1016/j.mssp.2021.106362.
23. Ningthemcha, R.K.N.; Mondal, R.; Das, A.S.; Debnath, S.; Kabi, S.; Singh, L.S.; Biswas, D. The effect of transition metal and heavy metal incorporation on the structural, optical and electrical properties of zinc-phosphate ternary glassy system: A comparative study. *Materials Chemistry and Physics* **2022**, *278*, https://doi.org/10.1016/j.matchemphys.2021.125672.
24. Ibrahim, A.M. Impact of MoO3 concentration, frequency and temperature on the dielectric properties of zinc phosphate glasses. *Chinese Journal of Physics* **2020**, *68*, 919–929, https://doi.org/10.1016/j.cjph.2020.07.013.
25. Assad, H.; Kharroubi, M. Dielectric studies and Cole-Cole plot analysis of $Na_2O$ – (1-x)ZnO –xCoO –$P_2O_5$ glasses. *Journal of Non-Crystalline Solids* **2021**, *560*, https://doi.org/10.1016/j.jnoncrysol.2021.120721.
26. Almuqrin, A.H.; Sayyed, M.I.; Kumar, A. Dielectric constant, polarizability, susceptibility and gamma ray shielding behavior of the $Li_2O$-$Li_2MoO_4$-$TiO_2$-$P_2O_5$ glasses. *Optik* **2021**, *245*, https://doi.org/10.1016/j.ijleo.2021.167639.
27. Mokhtar, K.; Mohamed, K.; Lakhdar, G.; Sébastien, B.; Hamza, A. Electrical conductivity and dielectric properties of rare earth ions ($Ce^{3+}$, $Pr^{3+}$ and $Eu^{3+}$) doped in zinc sodium phosphate glass. *Journal of Non-Crystalline Solids* **2021**, *567*, https://doi.org/10.1016/j.jnoncrysol.2021.120933.
28. El-Damrawi, G.; Abdelghany, A.M.; Madshal, M.A. AC conductivity and dielectric properties of $Cr_2O_3$ doped SrO–$P_2O_5$ glasses. *Physica B: Condensed Matter* **2021**, *618*, https://doi.org/10.1016/j.physb.2021.413184.
29. Hsouna, N.; Mhadhbi, M.; Bouzidi, C. Thermal and Electrical Characterization of (1-x)$Na_2O$-x$Al_2O_3$-$P_2O_5$ System Glasses. *Iranian Journal of Materials Science and Engineering* **2022**, *19*, 1–14, https://doi.org/10.22068/ijmse.2413.
30. Lograd, M.; Eckert, H.; Ikeda, H.; Nakane, S.; Yamazaki, H. Silica incorporation into sodium aluminum phosphate glasses: Structural characterization by Raman spectroscopy and multinuclear solid-state NMR. *Journal of Non-Crystalline Solids* **2022**, *579*, https://doi.org/10.1016/j.jnoncrysol.2021.121366.
31. Wang, F.; Wang, Y.; Zhang, D.; Hao, Y.; Liao, Q.; Zhu, H.; Zhou, J.; Zhu, Y. Effects of $MoO_3$ and Nd2O3 on the structural features, thermal stability and properties of iron-boron-phosphate based glasses and composites. *Journal of Nuclear Materials* **2022**, *560*, https://doi.org/10.1016/j.jnucmat.2021.153500.
32. Takebe, H.; Fujisawa, M.; Maeda, Y.; Saitoh, A. Effect of molybdenum oxide addition on the durability and structure of iron phosphate glasses. *Journal of Non-Crystalline Solids* **2021**, *129*, 105–110, http://doi.org/10.2109/jcersj2.20199.
33. Sayed, M.A.; Ali, A.M.; Abd El-Rehim, A.F.; Abdel Wahab, E.A.; Shaaban, K.S. Dispersion Parameters, Polarizability, and Basicity of Lithium Phosphate Glasses. *Journal of Electronic Materials* **2021**, *50*, 3116–3128, https://doi.org/10.1007/s11664-021-08921-9.
34. Kiwsakunkran, N.; Chanthima, N.; Kaewkhao, J.; Sangwaranatee, N. Fabrication of potassium aluminium barium phosphate glasses doped with $Sm^{3+}$ and their Judd-Ofelt analysis for orange lasing material application. *Materials Today: Proceedings* **2021**, *43*, 2554–2562, https://doi.org/10.1016/j.matpr.2020.04.616.

35. Pershina, S.V.; Antonov, B.D.; Leonidov, I.I. Effect of $MoO_3$ on structural, thermal and transport properties of lithium phosphate glasses. *Journal of Non-Crystalline Solids* **2021**, *569*, https://doi.org/10.1016/j.jnoncrysol.2021.120944.
36. Šantić, A.; Nikolić, J.; Renka, S.; Pavić, L.; Mošner, P.; Koudelka, L.; Tricot, G.; Moguš-Milanković, A. A versatile role of $WO_3$ and $MoO_3$ in electrical transport in phosphate glasses. *Solid State Ionics* **2022**, *375*, https://doi.org/10.1016/j.ssi.2021.115849.
37. Al-Buriahi, M.S.; Eke, C.; Alrowaili, Z.A.; Al-Baradi, A.M.; Kebaili, I.; Tonguc, B.T. Optical properties and radiation shielding performance of tellurite glasses containing $Li_2O$ and $MoO_3$. *Optik* **2022**, *249*, https://doi.org/10.1016/j.ijleo.2021.168257.
38. Wang, Y.; Wang, F.; Zhou, J.; Zhu, H.; Liao, Q.; Li, L.; Zhu, Y.; Yuan, Y.; Zhang, J. Effect of molybdenum on structural features and thermal properties of iron phosphate glasses and boron-doped iron phosphate glasses. *Journal of Alloys and Compounds* **2020**, *826*, https://doi.org/10.1016/j.jallcom.2020.154225.
39. Chatterjee, A.; Majumdar, S.; Ghosh, A. Effect of network structure on dynamics of lithium ions in molybdenum phosphate mixed former glasses. *Solid State Ionics* **2020**, *347*, https://doi.org/10.1016/j.ssi.2020.115238.
40. Baynton, P.L.; Rawson, H.; Stanworth, J.E. Glass based on the oxides of molybdenum, tungsten and uranium. *Nature* **1956**, *178*, 910–911, https://doi.org/10.1038/178910a0.
41. Goumeidane, F.; Legouera, M.; Iezid, M.; Poulain, M.; Nazabal, V.; Lebullenger, R. Synthesis and physical properties of glasses in the $Sb_2O_3$-$PbCl_2$-$MoO_3$ system. *Journal of Non-Crystalline Solids* **2011**, *357*, 3572–3577, https://doi.org/10.1016/j.jnoncrysol.2011.07.012.
42. Wu, X.; Zhao, S.X.; Yu, L.Q.; Li, J.W.; Zhao, E.L.; Nan, C.W. Lithium storage behavior of $MoO_3$–$P_2O_5$ glass as cathode material for Li-ion batteries. *Electrochimica Acta* **2019**, *297*, 872–878, https://doi.org/10.1016/j.electacta.2018.12.039.
43. Koudelka, L.; Rösslerová, I.; Holubová, J.; Mošner, P.; Montagne, L.; Revel, B. Structural study of PbO-$MoO_3$-$P_2O_5$ glasses by Raman and NMR spectroscopy. *Journal of Non-Crystalline Solids* **2011**, *357*, 2816–2821, https://doi.org/10.1016/j.jnoncrysol.2011.03.006.
44. Koudelka, L.; Kalenda, P.; Holubová, J.; Mošner, P.; Montagne, L.; Revel, B. Structural study of BaO-$MoO_3$-$P_2O_5$ glasses by Raman and NMR spectroscopy. *Journal of Non-Crystalline Solids* **2017**, *476*, 114–121, https://doi.org/10.1016/j.jnoncrysol.2017.09.040.
45. Šubčík, J.; Koudelka, L.; Mošner, P.; Montagne, L.; Tricot, G.; Delevoye, L.; Gregora, I. Glass-forming ability and structure of ZnO-$MoO_3$-$P_2O_5$ glasses. *Journal of Non-Crystalline Solids* **2010**, *356*, 2509–2516, https://doi.org/10.1016/j.jnoncrysol.2010.02.013.
46. Bih, L.; Abbas, L.; Nadiri, A.; Khemakhem, H.; Elouadi, B. Investigations of molybdenum redox phenomenon in $Li_2O$-$MoO_3$-$P_2O_5$ phosphate glasses. *Journal of Molecular Structure* **2008**, *872*, 1–9, https://doi.org/10.1016/j.molstruc.2007.02.005.
47. Lucacel, R.C.; Ponta, O.; Licarete, E.; Radu, T.; Simon, V. Synthesis, structure, bioactivity and biocompatibility of melt-derived $P_2O_5$ - CaO - $B_2O_3$ - $K_2O$ - $MoO_3$ glasses. *Journal of Non-Crystalline Solids* **2016**, *439*, 67–73, https://doi.org/10.1016/j.jnoncrysol.2016.02.022.
48. Rao, V.R.; Jayasankar, C.K. Spectroscopic investigations on multi-channel visible and NIR emission of $Sm^{3+}$-doped alkali-alkaline earth fluoro phosphate glasses. *Optical Materials* **2019**, *91*, 7–16, https://doi.org/10.1016/j.optmat.2019.02.007.
49. Unit, S.C. Characterization studies of molybdophosphate glasses and a model of structural defects. *Journal of Non-Crystalline Solids* **1985**, *72*, 315–334, https://doi.org/10.1016/0022-3093(85)90187-5.
50. Abbas, L.; Bih, L.; Nadiri, A.; Amraoui, Y. El; Khemakhem, H.; Mezzane, D. Chemical durability of $MoO_3$ – $P_2O_5$ and $K_2O$ – $MoO_3$ – $P_2O_5$ glasses. *Journal ofThermal Analysis and Calorimetry* **2007**, *90*, 453–458, https://doi.org/10.1007/s10973-006-7673-4.
51. Laourayed, M.; El Moudane, M.; Khachani, M.; Boudalia, M.; Guenbour, A.; Bellaouchou, A.; Zarrouk, A. Thermal, structural and corrosion inhibition performances of a new phosphate glasses on mild steel in HCl medium. *Chemical Data Collections* **2019**, *24*, https://doi.org/10.1016/j.cdc.2019.100305.
52. Alaoui, Y.; Moudane, M.E.; Er-Rafai, A.; Khachani, M.; Ghanimi, A.; Sabbar, A. Structural study, thermal and physical properties of $K_2O$-CaO-$P_2O_5$ phosphate glasses. *Moroccan Journal of Chemistry* **2021**, *3*, 454–463, https://doi.org/10.48317/IMIST.PRSM/MORJCHEM-V9I2.22505.
53. Little Flower, G.; Sahaya Baskaran, G.; Srinivasa Reddy, M.; Veeraiah, N. The structural investigations of PbO-$P_2O_5$-$Sb_2O_3$ glasses with $MoO_3$ as additive by means of dielectric, spectroscopic and magnetic studies. *Physica B: Condensed Matter* **2007**, *393*, 61–72, https://doi.org/10.1016/j.physb.2006.12.070.
54. Bartholomew, R.F. Structure and properties of silver phosphate glasses-Infrared and visible spectra. *Journal of Non-Crystalline Solids* **1972**, *7*, 221–235, https://doi.org/10.1016/0022-3093(72)90024-5.
55. Daasch, L.W.; Smith, D.C. Infrared Spectra of Phosphorus Compounds. *Analytical Chemistry* **1951**, *23*, 853–868, https://doi.org/10.1021/ac60054a008.
56. Ahmina, W.; El Moudane, M.; Zriouil, M.; Taibi, M. Glass-forming region, structure and some properties of potassium manganese phosphate glasses. *Phase Transitions* **2016**, *89*, 1051–1061, https://doi.org/10.1080/01411594.2016.1144057.

57. Brow, R.K.; Tallant, D.R.; Myers, S.T.; Phifer, C.C. The short-range structure of zinc polyphosphate glass. *Journal of Non-Crystalline Solids* **1995**, *191*, 45–55, https://doi.org/10.1016/0022-3093(95)00289-8.
58. Universitaire, D.; Elouadi, B.; Solid, A.; Chemistry, S.; Batota, A.I. Infrared spectra of vitreous lithium and cadmium mixed phosphates. *Canadian Journal of Chemistry* **1985**, *63*, 1436–1446, https://doi.org/10.1139/v85-247.
59. Liu, H.S.; Chin, T.S.; Yung, S.W. FTIR and XPS studies of low-melting PbO-ZnO-$P_2O_5$ glasses. *Materials Chemistry and Physics* **1997**, *50*, 1–10, https://doi.org/10.1016/S0254-0584(97)80175-7.
60. Salim, M.A.; Khattak, G.D.; Hussain, M.S. X-ray photoelectron spectroscopy, fourier transform infrared spectroscopy and electrical conductivity studies of copper phosphate glasses. *Journal of Non-Crystalline Solids* **1995**, *185*, 101–108, https://doi.org/10.1016/0022-3093(94)00683-0.
61. Omrani, R.O.; Krimi, S.; Videau, J.J.; Khattech, I.; El Jazouli, A.; Jemal, M. Structural investigations and calorimetric dissolution of manganese phosphate glasses. *Journal of Non-Crystalline Solids* **2014**, *389*, 66–71, https://doi.org/10.1016/j.jnoncrysol.2014.02.006.